Catalysis Letters
https://doi.org/10.1007/s10562-021-03750-1

PERSPECTIVE

Hydrogenomics: Efficient and Selective Hydrogenation of Stable Molecules Utilizing Three Aspects of Hydrogen

K. Fukutani[1,2] · J. Yoshinobu[3] · M. Yamauchi[4,5] · T. Shima[6,7] · S. Orimo[5,8]

Received: 9 May 2021 / Accepted: 18 July 2021

Abstract

Hydrogen is chemically flexible revealing three aspects; protium (H^0), proton (H^+), and hydride (H^-), which are active toward hydrogenation reactions. While the reactivity of protium is characterized by the potential energy at a catalyst surface, electron transfer is of importance as an additional degree of freedom in the reactions with proton and hydride. A promising strategy is to make full use of these active hydrogen species for hydrogenation of stable molecules and achieve chemical transformation of these molecules, which we call "Hydrogenomics". By reviewing recent studies on the hydrogenation of hydrocarbon, carbon dioxide, dinitrogen, and so on using these active hydrogen species on model metal surfaces, nanoscale electrocatalysts, and multimetallic polyhydride clusters, we discuss the fundamental concepts behind the reactions and possible control of the efficient and selective hydrogenation reactions.

Graphic Abstract

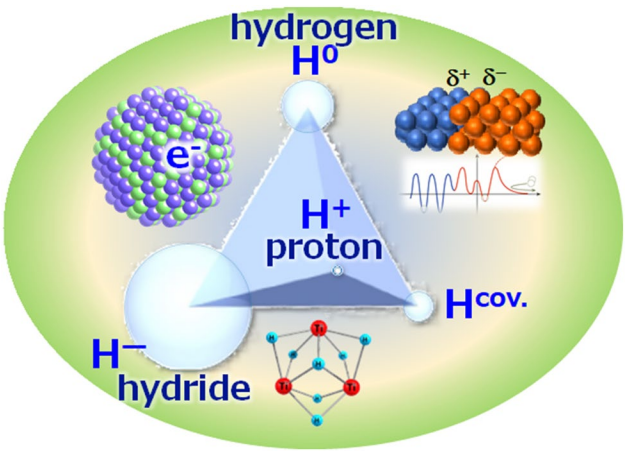

Keywords Hydrogenation · Processes and reactions, surface reaction kinetics · Elementary kinetics, electrocatalysis · Catalysis, hydride cluster, alloying

1 Introduction

Hydrogenation is an important chemical process to upgrade ubiquitous and stable chemical substances like dinitrogen and carbon dioxide to useful chemical feedstocks such as ammonia, hydrocarbons, alcohols among others. These chemical processes are closely related to environmental, energy and food problems. Molecular hydrogen consisting of two covalently bonded hydrogen atoms (H^{cov}) nonetheless electronically has a closed-shell structure like rare gas molecules thus being recognized as an inert molecule. When it is dissociated, on the other hand, the atomic hydrogen (protium, H^0) is

✉ K. Fukutani
fukutani@iis.u-tokyo.ac.jp

Extended author information available on the last page of the article

Published online: 30 July 2021

reactive toward various reactions. Since hydrogen has an intermediate electronegativity value, furthermore, hydrogen exhibits two other aspects of proton and hydride as shown in Fig. 1: Hydrogen possibly behaves as either positively charged proton (H^+) or negatively charged hydride (H^-) depending on its surrounding chemical environments [1]. This chemical flexibility grants us a powerful degree of freedom of the electronic energy to control the reactivity of hydrogen allowing for three approaches for hydrogenation reactions. Our strategy is to make full use of these active hydrogen species for hydrogenation of stable molecules and achieve chemical transformation of these molecules, which we call "Hydrogenomics".

A typical playground of protium is a metal surface, where atomic hydrogen is produced through dissociation of molecular hydrogen and simultaneously reactant molecules are accommodated for a subsequent reaction. The reactivity of protium depends on its site and the countermetal species of the surface, which is characterized by the potential energy corresponding to the enthalpy of the system. Controlled alloying is an effective approach to control the potential energy of the protium thereby allowing to tailor the reactivity of the hydrogen, which are discussed in Sect. 2.

Hydrogenation via proton is realized under electrochemical conditions. Whereas an electron is supplied from the cathode, a proton is delivered from the anode of the electrochemical circuit. In contrast to the enthalpy control for the reaction via the protium at a surface, the electronic potential can be tuned at a desired level to achieve selective and efficient reactions. By furthermore combining with alloyed electrodes, the electronic level can be effectively modulated enabling selective electron transfer to a reactant molecule thereby achieving highly selective hydrogenation reactions, typical examples of which are detailed in Sect. 3. In electrochemical hydrogenation reactions (EHR), possible use of renewable-energy-based electricity is also a considerable merit.

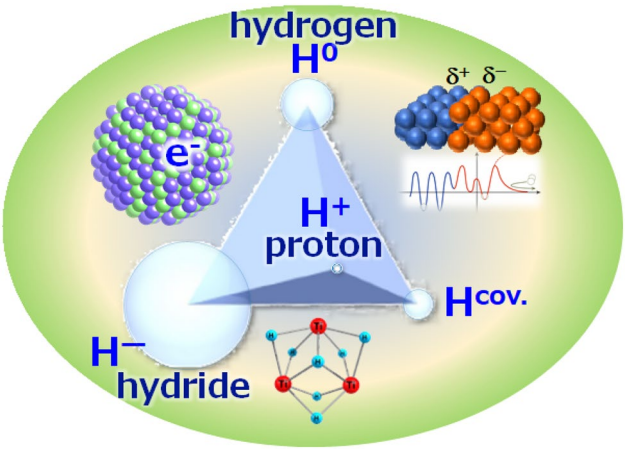

Fig. 1 Schematic illustration of three hydrogen states

Metal hydrogen compounds often offer hydride species for hydrogenation reactions and chemical transformations of reactant molecules [2]. The early transition metal-bonded hydrogen atoms exist in a negatively charged H^- state and readily transfer the multiple electrons to reactant molecules, which make significant contribution to the unsaturated-bond reduction and hydrogenation of reactant molecules. The high reactivity of hydrides is not only due to the nucleophilicity and basicity of the hydride species, but also the Lewis acidity and heteroatom (e.g., N, O, P,...) affinity of the metal centers. Multimetallic polyhydride clusters are of particular importance as they show synergistic effects on multimetallic reaction field, which enable the activation of chemically stable molecules transforming into useful chemical feedstocks as described in detail in Sect. 4.

Our world confronts serious environmental, energy and food problems in recent years. The relevant molecules are CO_2, N_2, CH_4 and so on, and chemical conversion of these molecules to useful chemical feedstocks is a vital challenge for chemists. To this end, making full use of the three hydrogen species in controlled manners is strongly desired. In this article, we introduce recent studies on the hydrogenation of some molecules such as hydrocarbon, carbon dioxide, and dinitrogen on model metal surfaces, nanoscale electrocatalysts, and multimetallic polyhydride clusters using the three reactive hydrogen species of $H^+/H^0/H^-$, and discuss the fundamental concepts behind the reactions and possible control of the efficient and selective hydrogenation reactions.

2 Potential-Energy Control of Protium at a Metal Surface

Molecular hydrogen tends to dissociate on transition metal surfaces producing atomic hydrogen on the surface. In order to precisely control surface reactions with high activity and selectivity by utilizing atomic hydrogen adsorbed on the surfaces, it is necessary to understand the potential energy surface (PES) of adsorption, diffusion and absorption of hydrogen on solid surfaces [3]. For this purpose, the preparation of a well-defined single-crystal surface as a model catalyst and the application of surface science techniques are quite effective.

Two typical types of the potential energy surface are displayed in Fig. 2 for dissociative adsorption and absorption of hydrogen on a metal surface. Figure 2a shows a potential energy curve of molecular hydrogen incident on a metal surface where the activation energy for dissociation is negligibly small (or zero). The dissociated hydrogen atoms adsorb on the surface and/or subsurface sites (exothermic process). In this figure, we assume that the enthalpy change

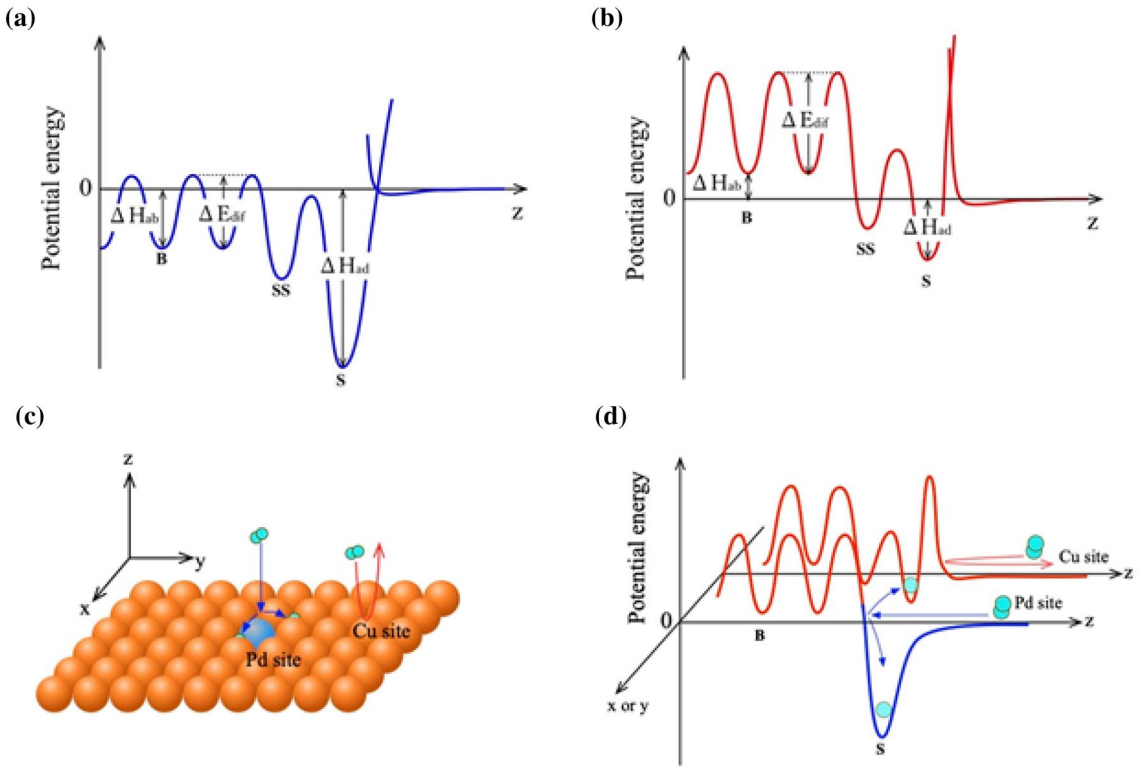

Fig. 2 **a** Potential energy diagram for dissociative adsorption and absorption of hydrogen with a negligible dissociation barrier. ΔH_{ad}: enthalpy change for hydrogen adsorption, ΔH_{ab}: enthalpy change for hydrogen absorption, ΔE_{dif}: activation barrier for bulk diffusion. *S* surface, *SS* subsurface, *B* bulk. **b** Potential energy diagram for dissociative adsorption of hydrogen with a high dissociation barrier **c** Schematic model of a single atom alloy surface, where an active Pd atom is embedded on the Cu surface. H_2 is dissociated at a Pd site but not at a Cu site. **d** Potential energy diagram of dissociative adsorption and absorption of hydrogen at the Pd and Cu sites

for absorption into the bulk is also negative (exothermic). A typical substance with this potential energy surface is Pd. In Fig. 2b, on the other hand, dissociative adsorption is highly activated indicating the dissociation of molecular hydrogen does not spontaneously occur under conventional conditions. However, once the dissociation occurs, the dissociated atomic hydrogen can be chemisorbed on the surface with a negative enthalpy change (exothermic) in adsorption on a surface, while the enthalpy change in absorption into the bulk is positive (endothermic). A typical substance in this case is Cu. In the following, we discuss how we can control the PES of hydrogen on metal surfaces.

2.1 Surface Alloy Formation for Potential Modulation

The use of alloys is one of the promising approaches to control the activation energy of dissociation of a hydrogen molecule, the adsorption and absorption energy of protium, and the activation energy of diffusion in the surface and bulk of hydrogen atoms. This is the most realistic and flexible strategy to control the states of hydrogen on metallic heterogeneous catalysts as Hydrogenomics. Alloys have long been used to enhance the functionality of catalysts [4]. However, it is rather difficult to elucidate the details of local structures and the electronic states of supported alloy catalysts. Surface science approaches allow us to intentionally supply heterogeneous atoms onto a single-element metal substrate for the fabrication of a well-defined bimetallic alloy model catalyst, and one can investigate the structure and properties of surface alloys on atomic scale.

Recently, single atom alloy catalysts (SAAC) have attracted much attention from both fundamental and applied point of view [5]. In particular, Sykes et al. have developed and investigated well-defined SAAC, which are tailored by depositing catalytically active atoms (Pt, Pd, Ni etc.) on more inert but more selective single-crystalline metal substrates (Cu, Ag, and Au) [6, 7]. Various surface science techniques including spectroscopy and microscopy have been applied to the well-defined SAAC surfaces in order to elucidate the structure, property and reaction on these surfaces on an atomic scale.

An interesting example of SAAC is reported by Kryakou et al. where a SAAC Pd-Cu(111) was successfully prepared by Pd deposition on a Cu(111) surface at 380 K in an ultra-high vacuum (UHV) [8]. Under this condition, Pd atoms

replaced Cu atoms at the surface, resulting in a model SAAC as shown in Fig. 2c. When hydrogen was introduced onto the surface at low temperature (80 K), the dissociation of a hydrogen molecule occurs at the Pd site. With increasing hydrogen exposure, adsorbed hydrogen atoms spill over to the Cu sites. These processes have been successfully observed on an atomic scale by scanning tunneling microscopy (STM) [8]. Figure 2d schematically shows the local potential energy surface at each site. Since the potential energy of protium on the Cu (111) surface is higher than that on the Pd surface, styrene and acetylene which are weakly adsorbed on the Cu surface at low temperature are selectively hydrogenated to ethylbenzene and ethylene, respectively. Whereas the Pd atoms play the role of dissociating molecular hydrogen, the Cu sites offer efficient reaction sites for hydrogenation reactions. In addition, vibrational spectroscopies including infrared reflection absorption spectroscopy (IRAS) [9] and high-resolution electron energy loss spectroscopy (HREELS) [10] and element-specific high-resolution core-level spectroscopy [11, 12] have been applied to elucidate the chemical properties of various SAAC surfaces.

There is a different approach to control the PES by depositing a low-activity metal on a high-activity metal surface to fabricate a surface alloy. While Au is inactive, Pd is active for hydrogen dissociation and absorption. Namba et al. fabricated a surface alloy by depositing Au atoms on a Pd(110) surface [13]. They demonstrate that the alloying the Pd(110) surface with submonolayer amounts of Au dramatically accelerates the hydrogen absorption by a factor of more than 40. First-principles calculations and photoelectron spectroscopy revealed that alloying the surface with Au raises the potential energy of adsorbed hydrogen and thus lowers the energy barrier (diffusion barrier) that hydrogen must cross to enter the bulk (Fig. 3). This is a successful example of the engineering of potential energy surface by surface alloying from the Hydrogenomics point of view.

As seen in these studies, alloying has two distinct aspects: combination of individual functions of constituent elements as demonstrated in the former, and modification of the original function of the host element.

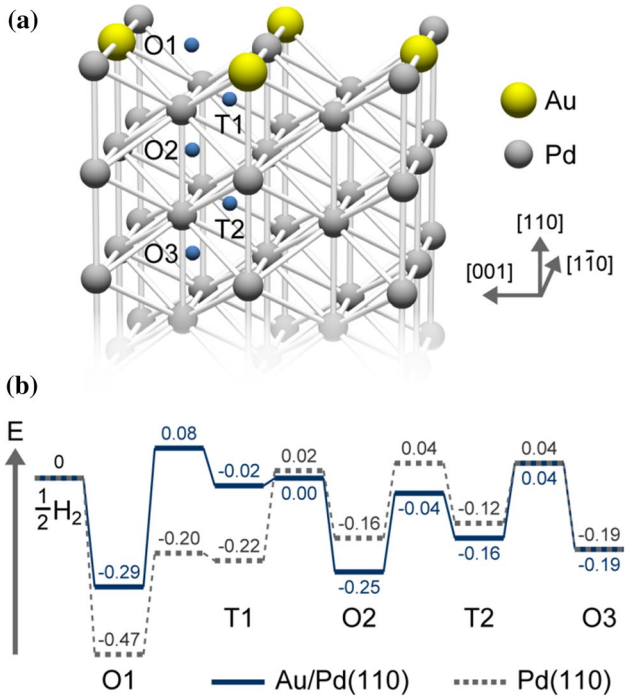

Fig. 3 **a** Schematic model of the 0.5 ML Au/Pd(110) used for DFT calculations. **b** Potential energy diagrams for a single H atom across the (solid line) 0.5 ML Au/Pd(110) and (dotted line) Pd(110) surfaces. The energies are shown in eV. Reprinted with permission from Ref. [13]

2.2 Subsurface Hydrogen

The protium residing at a subsurface site or absorbed in a bulk has a higher potential energy than that adsorbed on the surface (see Fig. 2a). When the absorbed protium is engaged in surface reactions without dissipating its energy across the surface, it could show higher activity and/or selectivity in catalytic reactions. Previously, Ceyer et al. demonstrated that hydrogen emerging from the subsurface sites of Ni(111) reveals the particular reactivity for the hydrogenation of adsorbed hydrocarbons, because the subsurface hydrogen in Ni is a strongly endothermic state [14]. Ohno et al. investigated the catalytic hydrogenation of cis-2-butene (C_4H_8) to butane (C_4H_{10}) by absorbed protium in Pd bulk using temperature-programmed desorption (TPD), HREELS, and nuclear reaction analysis (NRA) measurements [15]. They elucidated that the catalytic butene hydrogenation was initiated by the emergence of protium from the bulk Pd site onto the surface. Recently, Ogura et al. investigated the H–D exchange mechanism of butene on the D-absorbed PdAu alloy substrate [16] using TPD and HREELS [17]. They have demonstrated that both butene isomers are in the π-bonded states and that 1-butene irreversibly converts to cis-2-butene. Since the reverse change from cis-2- to 1-butene was not observed at any temperature, the H–D exchange proceeds by the dissociative mechanism via vinylic and π-allylic intermediates (Fig. 4). This conclusion does not agree with the traditional Horiuti–Polanyi mechanism [18], where hydrogenation and H–D exchange reactions of alkene often proceed via half-hydrogenated (C_nH_{2n+1}) and half-deuterated ($C_nH_{2n}D$) intermediates. As demonstrated in these studies, leveraging subsurface hydrogen as well as surface-adsorbed hydrogen allows us to explore new reaction routes due to the higher potential energy.

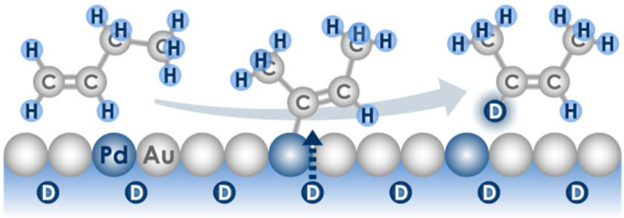

Fig. 4 Schematic illustration of the isotope exchange reaction for butene molecules via subsurface hydrogen. Reprinted with permission from Ref. [17]

2.3 Methanol Synthesis from CO_2

From the global environmental and ecological point of view, one of the most demanding and important catalytic reactions involving protium is the hydrogenation of CO_2 into methanol. At the present moment, methanol has been industrially synthesized with syngas via the reaction of $CO + 2H_2 \rightarrow CH_3OH$ using the $Cu/ZnO/Al_2O_3$ catalyst; this reaction is exothermic ($\Delta H = -90.7$ kJ/mol) and higher pressure is required from a chemical equilibrium point of view [19]. Methanol is an important chemical feedstock in a liquid form, which is possibly produced with renewable energy and is converted to a variety of chemical products including formaldehyde, acetic acid, methyl tert-butyl ether and so on [20]. The reuse of CO_2 is one of carbon neutral policies, i.e., a way to reduce CO_2 emissions. The conversion of CO_2 to methanol by hydrogenation would be one of the promising processes, and this reaction is described as $CO_2 + 3H_2 \rightarrow CH_3OH + H_2O$ ($\Delta H = -49.5$ kJ/mol). However, the synthesis of methanol from CO_2 has not been industrialized yet because the cost of CO_2 capture and H_2 production from renewable energy is higher than the cost using the syngas (CO and H_2) process from methane (natural gas; fossil feedstock) reforming as described above.

The methanol synthesis from CO_2 and H_2 consists of several elementary reactions on the Cu-based catalysts [21]. The elucidation of the reaction mechanism and the energy diagram including intermediate species and the activation barriers between them is still one of the advanced topics [22]. Recently, Quan et al. have reported the first step of this reaction, i.e., the formate species formation from a gaseous CO_2 molecule and an adsorbed hydrogen atom on a Cu surface [23]. They have elucidated that a vibrationally excited CO_2 molecule directly attacks a hydrogen atom on the Cu surface (Eley–Rideal type reaction), where the O=C=O bending motion plays an important role to react with the adsorbed hydrogen. By bending the O=C=O bond, the lowest unoccupied molecular orbital (LUMO) of CO_2 is decreased in energy according to the Walsh diagram [24], and thus the charge transfer from an electron-rich species to the C atom in CO_2 would more likely occur. In homogeneous catalytic reactions, the mechanism of direct CO_2 insertion into a Cu–H bond in the copper hydride complexes was proposed by quantum chemical calculations [25]. The adsorbed protium on Cu is relatively high in the potential energy, and it could show a hydride-like chemical reactivity.

Recently, indium oxide has been attracting much attention as an excellent catalyst for methanol synthesis from CO_2 [26], because In-based catalysts have lower catalytic activity for the reverse water gas shift reaction, $CO_2 + H_2 \rightarrow CO + H_2O$ ($\Delta H = 41.2$ kJ/mol) and consequently higher selectivity for methanol synthesis compared to the Cu/ZnO-based catalysts [27]. Nitrogen-doped Co nanosheets were found to show an improved catalytic reactivity for CO_2 hydrogenation, where Co_4N nanosheets were reconstructed into Co_4NH_x; the amido-hydrogen atoms directly interacted with the CO_2 to form HCOO intermediates [28]. On the whole, the development of multi-element component catalysts (alloy, intermetallic compound, SAAC etc.) is the key to control the local electronic states of adsorbed hydrogen and the reactant molecules resulting in more effective and selective catalytic reactions for desired products.

3 Nanoscale Electrocatalysts to Promote Electrochemical Hydrogenation by Activating Proton Functions

In electrochemical hydrogenation reactions, i.e., EHRs, water can be used as a hydrogen source and electrons and protons are produced via an electrooxidation of water at an anode. Then, electrons and protons are separately supplied to a reactant molecule from the cathode and anode, respectively. Thus, the efficient electron transfer from the electrode and controlled addition of protons to the reactant molecule determines catalytic performance, which invokes Hydrogenomics for the hydrogenation under mild conditions. By introducing recent studies on EHRs using metallic nanoalloys and modified TiO_2 as electrodes, we discuss rational design of nanoscale inorganic catalysts to enhance not only the catalytic activity but also product selectivity in EHRs. TiO_2 has been used as a photocatalyst to produce hydrogen via water decomposition [29] and recently is applied to EHRs [30]. Unlike metal electrodes, TiO_2 shows a high overpotential for hydrogen evolution, which improves the selectivity for the target chemicals. Whereas TiO_2 EHRs are applied to production of functional chemicals such as amino acids from bio-derivable organic acids [31], alloying an oxide with a foreign element furthermore induces unexpected reactivity in EHRs.

3.1 CO_2 EHRs on Metallic Nanoalloys for the Selective Production of Useful Chemicals

The efficiency for EHRs of CO_2 is markedly improved by collaborative developments of intensive experiments [32, 33] and mechanism elucidation [34]. When CO_2 is hydrogenated, a variety of products including formic acid, H_2, CO and $HCOO^-$ are possibly produced. Hori clarified that the product selectivity in EHRs largely depends on the metal catalysts [32]. Whereas Cu shows exceptional abilities in CO_2 EHRs [35], alloying with other metals such as Pd allows us to control the product selectivity by modulating the binding energy of intermediate species on the catalyst surface. In the alloy catalyst, furthermore, the mixing pattern of constituent elements makes considerable influence on the product selectively [36]. Yamauchi prepared three types of Cu–Pd nanoalloy (NA) catalysts having different mixing patterns, i.e., disordered (or solid-solution), ordered (intermetallics) and phase-separated NAs with an elemental ratio of Cu:Pd=50:50. In the phase diagram of the Cu–Pd system, a B2-type ordered phase having a body-centered-cubic-like arrangement emerges at the proximate of Cu:Pd = 60:40. Hydrogen treatment enhances elemental diffusion via formation of vacancies in the NA lattice at temperatures much lower than the melting point. Thus, the B2-type CuPd ordered NAs were prepared by H_2 treatment of disordered ones [37].

Figure 5 shows Faradaic efficiencies (FE) for the products generated on CuPd NAs, which present the ratio of the electrons consumed for generation of each product and are related to the selectivity for the product, and reaction formulae with an equilibrium potential represented versus the reversible hydrogen electrode (RHE) [38]. On the ordered B2-type CuPd, CO was the main product (Fig. 5a) whereas C2 chemicals such as C_2H_4 and EtOH were mainly produced on the phase separated NAs (Fig. 5c). The disordered CuPd NAs showed an intermediate product distribution between B2 and phase separated ones (Fig. 5b). The FE for the production of C2 compounds on the disordered NAs was found to increase with increasing Cu concentration, whereas FE for CH_4 production becomes maximum on disordered CuPd NAs [38]. These results suggest that the dimerization of adsorbed CO to form C2 chemicals may be preferred on the Cu clustering site, and that isolated Cu sites favorably produce CH_4 in CO_2 EHRs. Furthermore, appropriate arrangement of catalytic sites for proton supply is also important. Interestingly, FEs for more hydrogenated products on CuPd NAs seem high, i.e., disordered CuPd NAs exhibit the highest CH_4 selectivity, probably because Pd sites efficiently provide protons to intermediate species. These results imply that the geometric arrangement of active sites as well as the alloy composition is a critical factor to determine the product selectivity in EHRs.

3.2 EHRs of Organic Acids on TiO_2-Based Oxide Electrodes for the Electric Power Storage into Liquid Fuels

EHRs realize direct electric power storage in high-energy chemicals or fuels with a minimum environmental load. Bio-derivable materials such as organic acids are essentially low-carbon chemical resources, because plants naturally accumulate atmospheric CO_2. Highly selective EHRs with a TiO_2 electrode was recently reported, where bio-derivable oxalic acid (HOOC–COOH, OX) was converted to glycolic acid (HOOC–CH_2OH, GC) in the following reaction scheme:

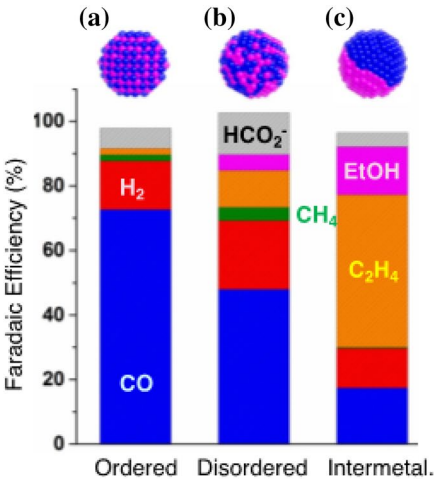

(d)

Reaction	^0E (V vs RHE)
$CO_2 + 2H^+ + 2e^- \rightarrow CO + H_2O$	-0.10
$2CO_2 + 12H^+ + 12e^- \rightarrow C_2H_4 + 4H_2O$	+0.08
$2CO_2 + 12H^+ + 12e^- \rightarrow C_2H_5OH + 3H_2O$	+0.09
$CO_2 + 8H^+ + 8e^- \rightarrow CH_4 + 2H_2O$	+0.17

Fig. 5 Faradaic efficiency for CO_2 EHRs on three types of **a** ordered B2-type, **b** disordered and **c** phase-separated CuPd nanoalloys (NAs). **d** Representative reaction formulae with equilibrium potentials vs. RHE

Cathode: $HOOC\text{-}COOH + 4H^+ + 4e^- \rightarrow HOOC\text{-}CH_2OH + H_2O$ + 0.13 V vs RHE

Anode: $2H_2O \rightarrow 4H^+ + 4e^- + O_2$ + 1.23 V vs RHE

Overall: $HOOC\text{-}COOH + H_2O \rightarrow HOOC\text{-}CH_2OH + O_2$ 1.1 V

In this EHR system, GC is produced via the 4-electron reduction of OX, which affords efficient electronic power storage into GC with a high volumetric energy density of 8600 MJm^{-3}, which is much higher than the value of 13 MJm^{-3} for H_2 gas.

Interestingly, furthermore, anatase TiO_2 is shown to be active whereas rutile TiO_2 is inactive toward the above reaction. As shown in Fig. 6a–f, electron energy loss spectroscopy (EELS) mapping measurements clarify that active TiO_2 is composed of anatase and inactive catalysts are covered with rutile TiO_2. The reason for the higher activity of anatase TiO_2 is attributed to the band structure, of which conduction band bottom is significantly higher than that of rutile and has an appropriately high energy level for OX EHR compared to that of rutile ones as shown in Fig. 6g [30].

A recent DFT study elucidates the three crucial factors for the promotion of electro-reduction of carboxylic acids: [40] (1) Semiconductor catalyst having a LUMO level sufficiently higher than the LUMO of a carboxylic acid, (2) Extension of the conjugation system around the carboxyl group of the reactant to stabilize transition states, and (3) Highly developed hybridization between LUMO of a reactant molecule and orbitals of the catalyst surface that enhances charge transfer from the electrode to the reactant. These results suggest that the relative energy positions of LUMOs of oxides and reactants significantly affect the activity in EHRs of organic acids.

Another approach to enhance the activity for OX reduction is alloying of TiO_2 with other elements [39]. A Zr ion exhibits a valence state similar to that of a Ti ion with a larger ionic radius than that of the Ti ion: the ionic radii of Zr^{4+} and Ti^{4+} ions are 0.720 and 0.605 Å, respectively. Ti–ZrO_2 complex oxide particles with an entire range of composition were prepared via a solvothermal method. All of the prepared $Ti_{(1-x)}Zr_xO_2$ particles showed spherical morphology similarly to TiO_2 as shown in Fig. 7. Up to x=0.15, the complex nanoparticles have the anatase structure and became amorphous in the x range from 0.2 to 0.8. Interestingly, both conversion of OX and FE for the production of GC depend on the x value as shown in Fig. 8. FEs for the GC production rapidly increased up to x=0.1 and decreased at x=0.15 suggesting that the crystal structure is related to

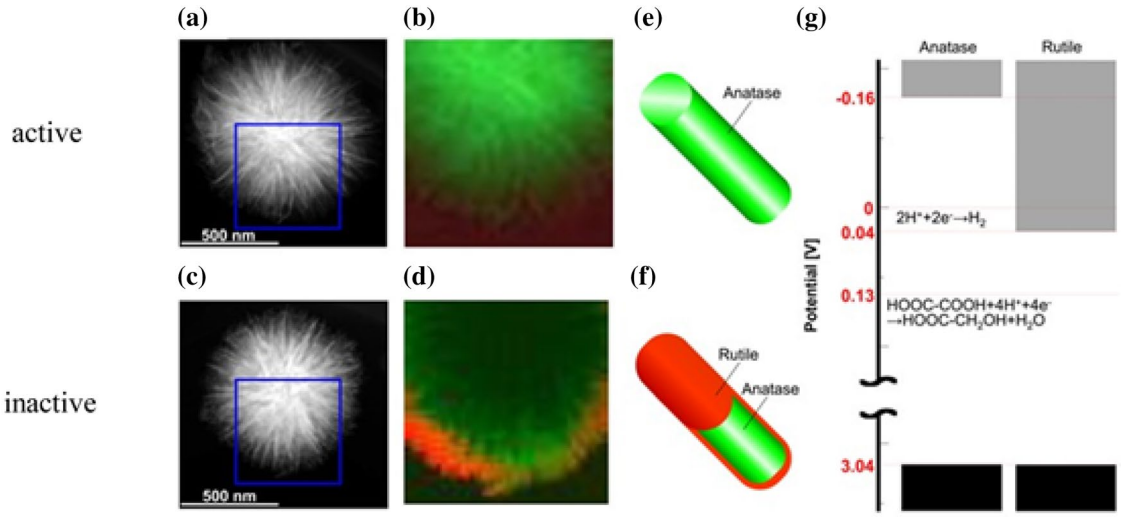

Fig. 6 **a** and **c** STEM images of active and inactive TiO_2 catalysts for EHRs of oxalic acid, respectively. **b** and **d** EELS maps of active and inactive catalysts composed of Ti L_3-edge signals in the area marked by blue squares in (**a**) and (**c**). The EELS signal intensities from the anatase and rutile phases are recognized by green and orange colours, respectively. Illustrations for distributions of anatase and rutile phases in (**e**) active and **f** inactive catalysts. **g** Energy diagrams of the conduction (grey) and valence (black) bands for anatase- and rutile-type TiO_2 assuming that the flat-band potential is equal to the conduction-band edge potential, and the redox potentials for the production of H_2 and GC. Reproduced from Ref. [30] with permission from The Royal Society of Chemistry

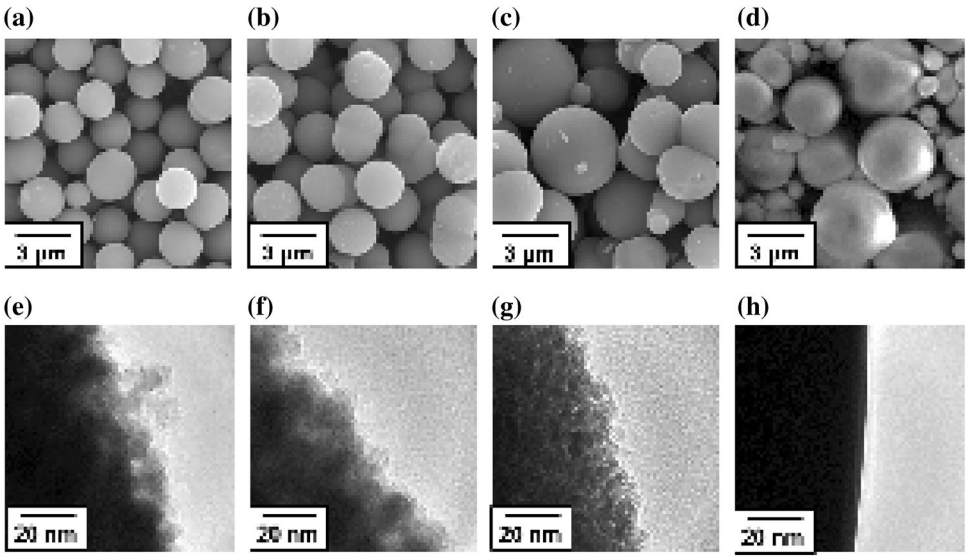

Fig. 7 SEM (upper) and TEM (lower) images for **a**, **e** TiO_2, **b**, **f** $Ti_{0.9}Zr_{0.1}O_2$, **c**, **g** $Ti_{0.75}Zr_{0.25}O_2$, **d**, **h** ZrO_2 particles. Reproduced from Ref. [39] with permission from the PCCP Owner Societies

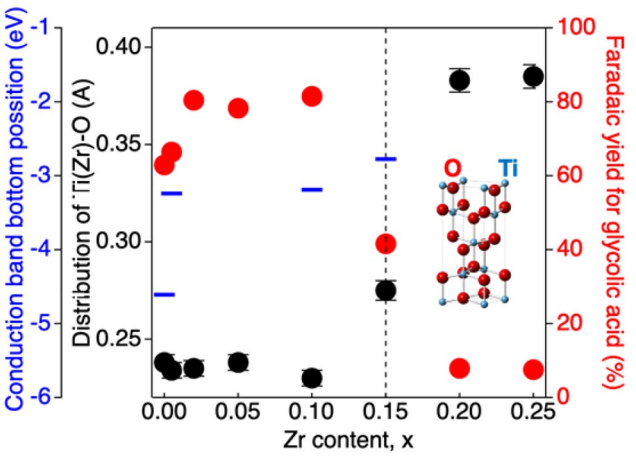

Fig. 8 Zr content (x) dependence of the Faradaic efficiency for GC productions on $Ti_{1-x}Zr_xO_2$ particles at − 0.7 V vs. RHE at 50 °C for 2 h (red, right), energy levels of the conduction band bottom of $Ti_{1-x}Zr_xO_2$ particles (blue, left) and the distribution of Ti(Zr)–O distances (black, left). Dotted lines indicate a boundary between the anatase and amorphous phases. Reproduced from Ref. [41] with permission from the PCCP Owner Societies

the OX EHR activity. To clarify the reason for the composition-dependent activity enhancement, the electronic states of $Ti_{(1-x)}Zr_xO_2$ particles were examined as shown in Fig. 8. It is noticeable that the energy level of the conduction band bottom (CBB) rapidly rises at x=0.05 and becomes constant above x=0.05. Thus, higher CBB levels seem advantageous to reduce reactants. The rapid decrease in FE around x=0.15, on the other hand, is attributed to the structural peculiarity. The local structures of the complex particles were investigated by the atomic pair distribution function (PDF) analysis of synchrotron X-ray total scattering [41]. Figure 8 also presents Zr-content dependence of the distribution of the distance between metal and O ions (M–O distance) and FEs for GC production. Surprisingly, FEs look well correlated with the M–O distance.

While the energy-level alignment is an important requisite for higher activity in OX EHRs, the geometric arrangement like the M–O distance is another crucial factor to accommodate molecular adsorption thereby significantly modifying the EHR activity.

3.3 EHR-Based Amination of Organic Acids on TiO_2 to Produce Amino Acids

EHRs combined with other chemical reactions enable us to produce complicated chemicals more than alcohols. Imines or oximes form via the reaction between α-keto acids and ammonia or hydroxylamine. EHRs of mixed solutions of α-keto acids and hydroxylamine realized the formation of corresponding amino acids with considerably high FEs, i.e., high selectivity as shown in Fig. 9 [31]. Recent DFT calculations have predicted that proton-coupled electron transfer, which couples with an oxide surface and reactants plays important roles [42]. Favorable hydrogen bonding networks remarkably stabilize the transition states for the N–H bond formation in alanine synthesis from oxime (Fig. 9b and c) compared to that in the hydrogen atom transfer. Since the research of EHRs using oxide electrodes is largely unexplored, further development of catalytic surfaces for efficient EHRs is highly awaited.

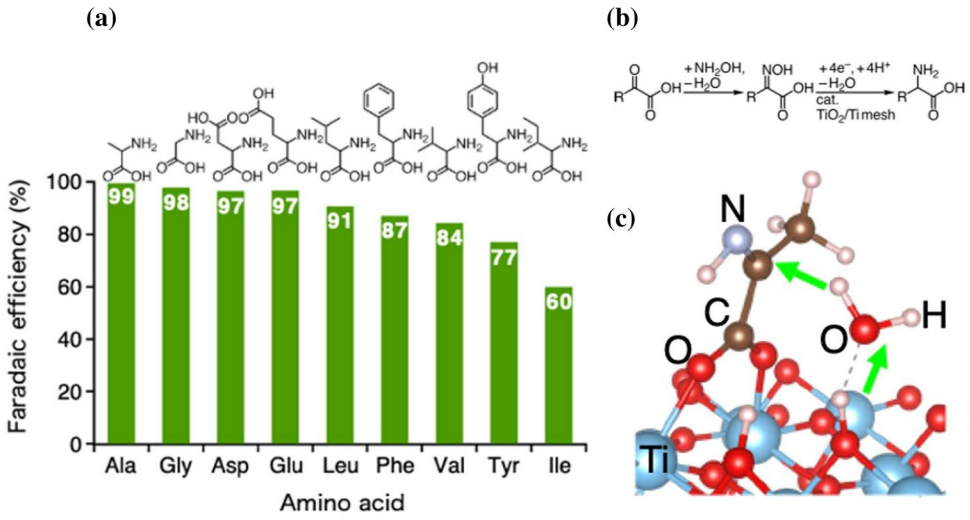

Fig. 9 **a** Faradaic efficiency for amino acid production via EHRs of corresponding oximes formed from α-keto acids with hydroxylamine. **b** Reaction scheme of amino acid production in the presence of hydroxylamine. **c** Graphitic scheme of proton coupled electron transfer for C–H bond formation in alanine formation. Green arrows indicate the direction of proton transfers

4 Small Molecule Activation and Transformation by Multimetallic Hydride Clusters

The last approach of the Hydrogenomics concept is utilization of hydride species on multimetallic polyhydride clusters for small molecule activation and transformation. One of the main synthetic routes to obtain multimetallic polyhydride clusters is hydrogenation of the metal alkyl precursors with H_2. Our previous studies have shown that the hydrogenolysis of the $C_5Me_4SiMe_3$-ligated half-sandwich rare-earth dialkyl complexes such as $[(C_5Me_4SiMe_3)Ln(CH_2SiMe_3)_2(THF)]$ (Ln = Sc, Y, and lanthanide metals) with H_2 could afford the corresponding tetranuclear rare-earth polyhydride clusters $[(C_5Me_4SiMe_3)_4Ln_4(\mu\text{-}H)_8(THF)]$ [43, 44], which showed high and unique reactivities toward various reactants through the cooperation of multiple Ln–H sites [45–47]. In the course of our studies on the $C_5Me_4SiMe_3$-ligated half-sandwich type polyhydride clusters, we have found that hydrogenolysis of the $C_5Me_4SiMe_3$-ligated titanium alkyl complex $[(C_5$

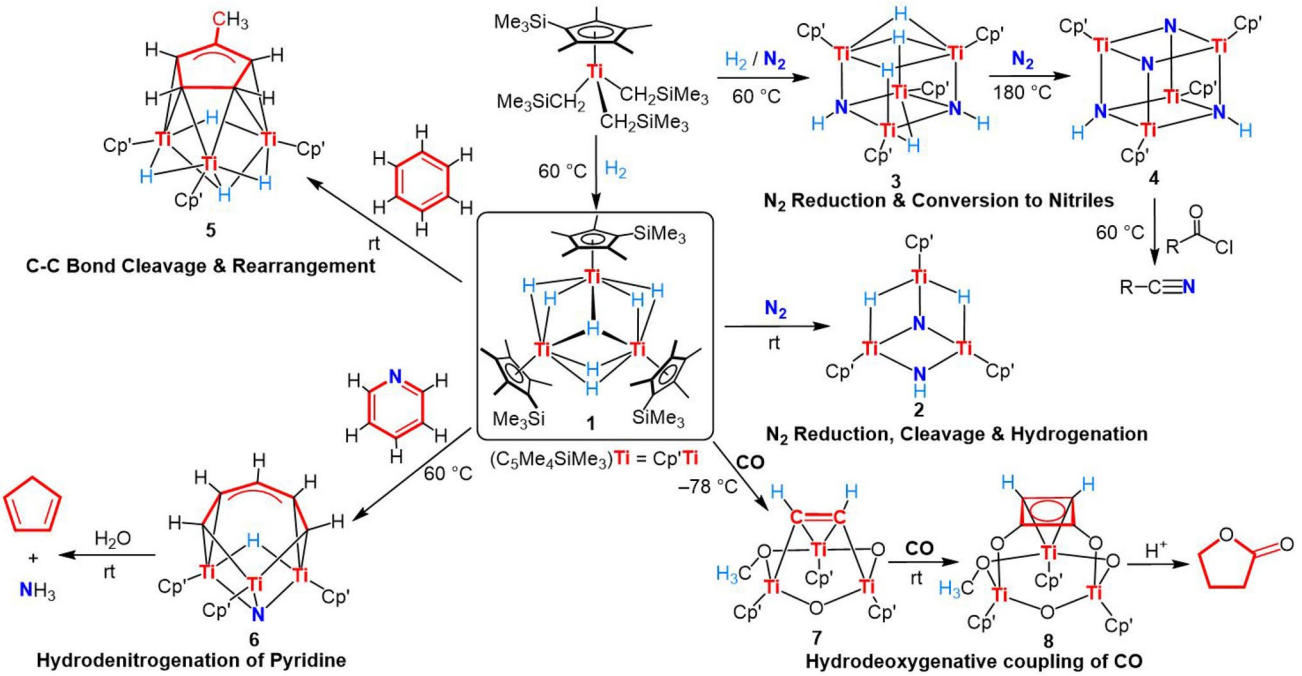

Fig. 10 Small molecule activation and transformation by a trinuclear hydride cluster 1, demonstrating the versatile roles of hydrides

Me_4SiMe_3)Ti(CH_2SiMe_3)$_3$] with H_2 afforded mainly the mixed valence Ti(III)/Ti(IV) heptahydride cluster [($C_5Me_4SiMe_3$)$_3$Ti$_3$(μ_3-H)(μ-H)$_6$] (1) (Fig. 10). This cluster 1 shows remarkable reactivity toward various small molecules under mild condition as detailed below (Fig. 10) [48, 49]. In addition to the Ti-based hydride cluster, $C_5Me_4SiMe_3$-ligated chromium hydride clusters are recently synthesized, which exhibits high reactivity toward N_2. These multimetallic polyhydride clusters show unique synergistic effects in the activation of small molecules through the cooperation of multiple M–H sites.

4.1 N_2 Cleavage and Hydrogenation by Titanium Hydride Clusters

There have been previous extensive studies on N_2 reduction via a combination of transition-metal complexes and strongly reducing metal reagents. In contrast to these methods, the N_2 reduction by transition metal hydrides offers a unique approach avoiding use of special reducing agents and proton sources. Cluster 1 readily reacts with N_2 (1 atm) at room temperature, giving an imide/nitride cluster [($C_5Me_4SiMe_3$)$_3$Ti$_3$(μ-NH)(μ_3-N)(μ-H)$_2$] (2) through N–N bond cleavage and N–H bond formation without the need of extra reducing agents or proton sources (Fig. 10) [50]. The hydride ligands in 1 served as the source of both electron and proton for the N_2 cleavage and hydrogenation.

The energetic profiles of the reaction of 1 with N_2 are clarified by DFT calculations on the basis of a model compound 1 (i.e., [($C_5H_4SiH_3$)$_3$Ti$_3$(μ-H)$_7$] (1m)) (Fig. 11). The reaction initially afforded the dinitrogen incorporated intermediate A without an energy barrier. The subsequent N–N bond cleavage (leading to B) and migration of the hydride ligand to the μ_2-nitride ligand afforded the monoimide/nitride product 2m. The rate-determining step of the whole transformation is the N–H bond formation step (26.5 kcal/mol).

Although well-defined transition-metal hydride complexes that enable N_2 activation and hydrogenation reported to date are still limited, the activation and hydrogenation of dinitrogen (N_2) by well-defined molecular transition-metal complexes is expected to help researchers better understand the N_2 transformation mechanism at the molecular level and thereby lead to the development of efficient catalysts for ammonia synthesis under mild conditions.

4.2 Conversion of N_2 to Nitriles

When hydrogenolysis of [($C_5Me_4SiMe_3$)Ti(CH_2SiMe_3)$_3$] with H_2 was carried out in the presence of N_2, a tetranuclear imide/hydride cluster [($C_5Me_4SiMe_3$)$_4$Ti$_4$(μ_3-NH)$_2$(μ-H)$_4$] (3) was obtained (Fig. 10) [50]. Further N_2 activation took place when heating 5 with N_2 at 180 °C, which afforded a mixed imide/nitride cluster [($C_5Me_4SiMe_3$)$_4$Ti$_4$(μ_3-NH)$_2$(μ_3-N)$_2$] (4) with a release of two H_2 molecules [51, 52]. Notably, the imide/nitride species in cluster 4 could be easily converted to nitriles via the reaction with acid chlorides RC(O)Cl at 60 °C. This protocol features simple reaction condition (60 °C in benzene), no requirement for extra reagents (either a reducing agent or Lewis acid or base), and unprecedented functional group tolerance (good compatibility with aromatic C–X (X = Cl, Br, I) bonds, nitro group, and ammonia-sensitive aldehyde and chloromethyl moieties).

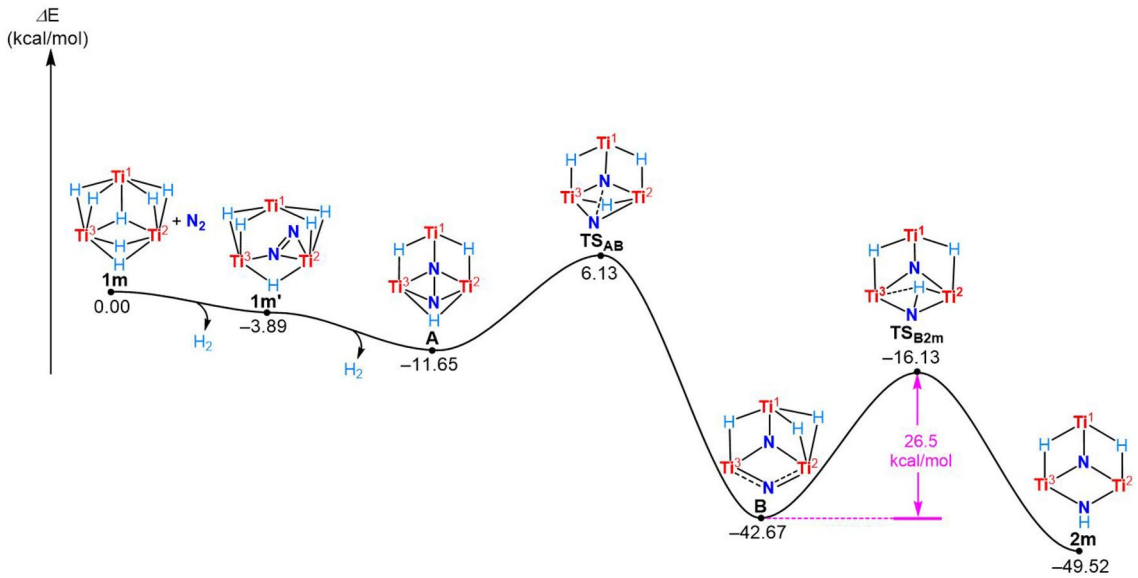

Fig. 11 DFT analysis of N_2 activation by 1m. Cyclopentadienyl ligands are omitted for clarity

At present, ammonia (NH_3), produced by the energy-intensive Haber-Bosch process, is the only nitrogen source for the industrial preparation of nitrogen-containing organic products. Although the activation and functionalization of N_2 under milder conditions have received much recent interest, studies on the direct use of N_2 as a feedstock for organic synthesis are still in their infancy. The above reaction offers a good opportunity to develop direct conversion of N_2 to N-containing organic compounds without using NH_3.

4.3 C–C Bond Cleavage and Rearrangement of Benzene

Cluster 1 shows unique reactivity toward aromatic compounds. When a benzene solution of 1 was kept at room temperature for a few days or at 40 °C for 36 h, a methylcyclopentenyl cluster $[(C_5Me_4SiMe_3)_3Ti_3(C_5H_4Me)(\mu\text{-}H)_4]$ (5) was formed quantitatively via C–C bond cleavage and rearrangement of benzene (Fig. 10) [53, 54]. Remarkably, a benzene molecule was partly hydrogenated and ring-rearranged from six to five-membered ring species. Further C–C bond cleavage took place when 5 was heated at 100 °C for 2 days, giving a titanacyclohexenyl cluster via insertion of a Ti atom into a C–C bond of the methylcyclopentenyl ring in 5.

Generally, the C–C bond is quite stable and is consequently unreactive under ordinary reaction conditions. Although some molecular transition metal complexes have been reported to cleave C–C bonds in a selective fashion under special circumstances, the cleavage of benzene by transition metal complexes has not been reported previously. The above results not only provide unprecedented insights into the activation and transformation of benzene over a multimetallic framework but may also offer help in the design of new molecular catalysts for the activation and transformation of inactive aromatics.

4.4 Hydrodenitrogenation of Pyridine

The hydrodenitrogenation (HDN) of N-heteroaromatics such as pyridines is an important process in the industrial petroleum refining to remove nitrogenous impurities from crude oil. Due to the stable C–N bonds of N-heteroaromatics, however, it is difficult to break the bonds under ordinary conditions. Cluster 1 can ring-open and denitrogenate pyridines under mild conditions (Fig. 10) [55]. The nitrogen atom in a pyridine ring was extruded through the dehydrogenative reduction of the C=N unit followed by cleavage of the two C–N bonds at a trimetallic titanium framework (leading to cluster 6). Both linear and cyclic nitrogen-free hydrocarbons such as cyclopentadiene were selectively generated from pyridines under appropriate conditions. This work represents the first example of HDN of N-heteroaromatics by a well-defined molecular system, and may help better understand the industrial HDN process and guide designing new catalysts.

4.5 Hydrodeoxygenative Coupling of CO

Cluster 1 shows hydrodeoxygenative cyclotetramerization of CO. When a THF solution of 1 was kept at − 78 °C under CO (1 atm) for 10 min, hydrodeoxygenative C–C coupling of CO took place to give an ethylene-bridged dioxy/methoxy cluster 7 (Fig. 10) [56]. When a THF solution of 7 was stirred under CO at room temperature for 12 h, a cyclobuten-3,4-diyl-1,2-diolate cluster 8 was obtained. The acidolysis of 8 with HCl afforded γ-butyrolactone together with methanol as an organic compound.

The hydrodeoxygenative coupling of carbon monoxide has attracted great attention because it can offer an intriguing route for the production of low molecular weight commodity chemicals and liquid fuels from easily accessible resources. As compared to the reaction with mononuclear metal complexes, CO reduction with multinuclear hydride clusters have remained much underexplored to date. This work demonstrates that a multimetallic titanium hydride cluster serves as a unique platform for CO transformation.

4.6 N_2 Activation by Chromium Hydride Clusters

For well-defined molecular Group 5 transition-metal hydride systems, Fryzuk and Kawaguchi reported some dinuclear group 5 transition-metal tantalum [57] and niobium [58–60], polyhydride complexes, which can reduce and split N_2. To date, well-defined transition-metal hydride complexes that enable N_2 cleavage and hydrogenation have been limited only to group 4 and 5 transition metals. Whereas some group 6 transition metal hydride complexes are known to trap N_2, significant reduction of a coordinated N_2 unit has not been observed. Very recently, $C_5Me_4SiMe_3$-ligated half-sandwich type multimetallic chromium polyhydride clusters were found to enable N_2 cleavage and hydrogenation under mild conditions without the need for any extra reagents.

Hydrogenolysis of the $C_5Me_4SiMe_3$-ligated chromium(II) methyl complex $[Cp'Cr(\mu\text{-}Me)]_2$ (9) ($Cp' = C_5Me_4SiMe_3$) in a dilute hexane solution with H_2 under N_2-free conditions at room temperature afforded a dinuclear Cr(II) dihydride cluster $[Cp'Cr(\mu\text{-}H)]_2$ (10) (Fig. 12) [61]. In contrast, when the reaction was carried out in a concentrated solution, a trinuclear mixed-valence Cr(II)/Cr(III) tetrahydride cluster $[(Cp'Cr)_3(\mu_3\text{-}H)(\mu\text{-}H)_3]$ (11) was formed exclusively. Heating a solid of 10 with H_2 at 50 °C also afforded 11.

Hydrogenolysis of the alkyl complex 9 in dilute hexane solution with a mixture of H_2 (4 atm) and N_2 (1 atm)

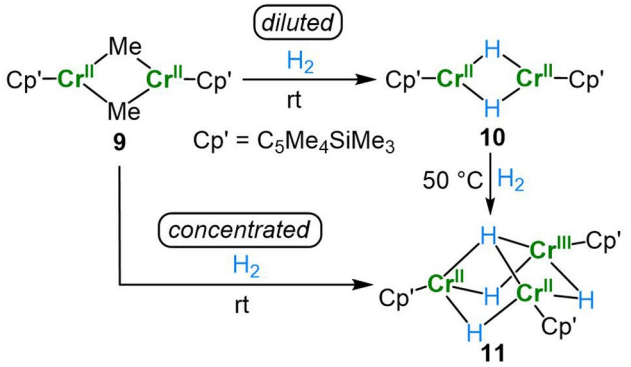

Fig. 12 Syntheses of the $C_5Me_4SiMe_3$-ligated chromium hydride clusters

at room temperature for 2 days afforded the tetranuclear diimide/dihydride complex $[(C_5Me_4SiMe_3)_4Cr_4(\mu_3\text{-}NH)_2(\mu_3\text{-}H)_2]$ (12) via N–N bond cleavage and N–H bond formation (Fig. 13) [61]. The dinuclear hydride 10 was found to serve as an active hydride species for this N_2 activation. When a hexane solution of 10 was kept under N_2 at − 30 °C, dark green crystals of a tetranuclear chromium dinitride/dihydride cluster $[(Cp'Cr)_4(\mu_3\text{-}N)_2(\mu_3\text{-}H)_2]$ (13) were obtained (Fig. 13). In this reaction, one N_2 molecule was split into two nitrido (N^{3-}) units by two molecules of 10 through release of one molecule of H_2 and oxidation of four Cr(II) to Cr(III). Cluster 13 was converted to diimide/

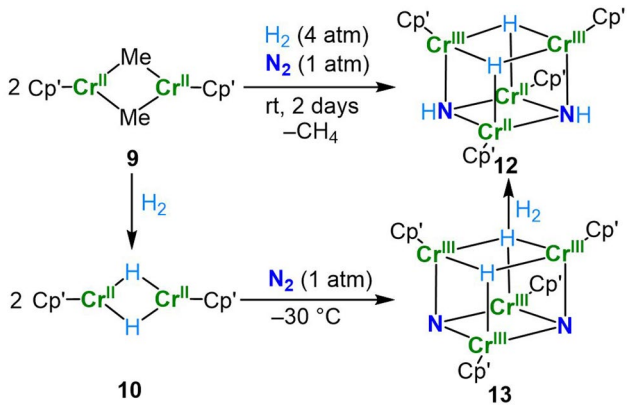

Fig. 13 N_2 activation and hydrogenation by a dinuclear chromium hydride cluster 10

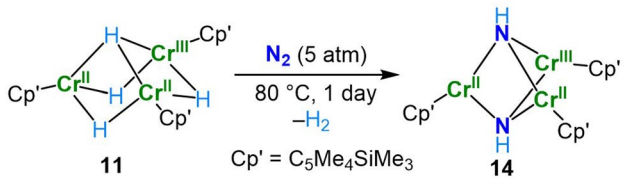

Fig. 14 N_2 activation and hydrogenation by a trinuclear chromium hydride cluster 11

hydride cluster 12 at room temperature under H_2 through the hydrogenation of the nitride unit in 13 (Fig. 13).

In addition to the dinuclear chromium dihydride cluster 10, the trinuclear chromium tetrahydride cluster 11 also activated N_2 at elevated pressure and temperature. When 11 was heated in hexane at 80 °C under N_2 (5 atm), N_2 cleavage and hydrogenation occurred to afford a diimide cluster $[(Cp'Cr)_3(\mu_3\text{-}NH)_2]$ (14) (Fig. 14).

According to the result of kinetic experiments and DFT calculations (Fig. 15), the reaction was initiated by N_2 coordination to a chromium atom (model compound ^{10}A), followed by H_2 elimination (^{10}B). The subsequent N–N bond cleavage (^{8}C) and two hydride transfer (^{10}D, ^{4}14m) to the two nitride ligands afforded the diimide product 14. Although the overall steps of the reaction of 11 with N_2 were comparable to those of 1 with N_2 (Fig. 11), its energy profiles (rate determining step: Cr, initial uphill N_2 incorporation and reduction step vs. Ti, N–H bond formation step) and final product (Cr, diimide cluster 14 vs. Ti, monoimide/mononitride cluster 2) were in contrast with those of the titanium cluster 1, reflecting the metal influence.

5 Summary and Outlook

We have reviewed and discussed recent studies on hydrogenation reactions with three types of active hydrogen species. In its atomic form, the reactivity is closely related to the potential energy of adsorbed and absorbed protium, which can be quantitatively described on well-defined surfaces. We have shown two approaches to modulate the PES by fabricating surface alloys on well-defined surfaces. In the former, by depositing active transition metal atoms (Ni, Pd, Pt etc.) on more inert but more reaction-selective metal substrates (Cu, Ag, Au, etc.), various single atom alloy catalysts (SAAC) have been developed for specific hydrogenation reactions with efficient dissociation of H_2 to adsorbed hydrogen atoms. In the latter, on the other hand, by depositing a low-activity metal such as Au on a high-activity metal substrate (Pd), the potential energy of adsorbed hydrogen is significantly raised thus decreasing the energy barrier for bulk diffusion, which dramatically accelerates the hydrogen absorption rate. Additionally, hydrogen atoms at subsurface and bulk sites, which have a higher potential energy, can be utilized to hydrogenation reactions on a catalyst surface as hot hydrogen atoms. Further development of multi-element alloy catalysts, which are precisely designed and fabricated from the viewpoint of the potential energy surface, is demanded for more effective and more selective heterogeneous catalytic reactions. It is also worth noting that the PES control is of relevance and importance for EHRs.

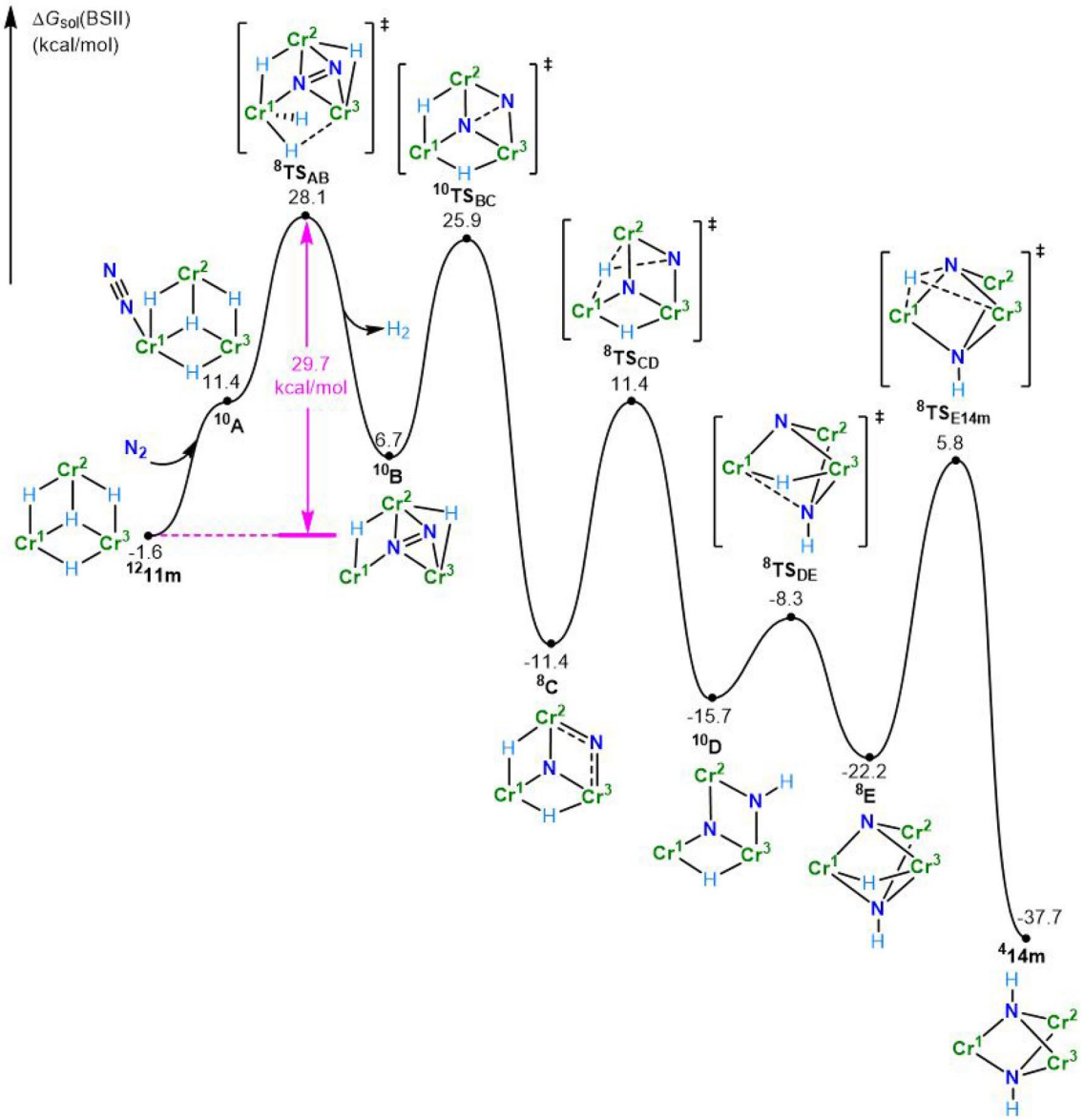

Fig. 15 DFT analysis of N_2 activation by 11 m. Cyclopentadienyl ligands are omitted for clarity. The left superscript denotes the spin multiplicity of the corresponding species (e.g., ^{4}14 m is a quartet)

Since protons and electrons are separately supplied in EHRs, the catalytic performance is correlated with the electronic state for electron transfer and the surface structure for proton transfer. In CO_2 EHRs, Cu exhibits high activity as an electrocatalyst and the degree of agglomeration of Cu on the catalyst surface is considerably reflected to the carbon number of the products. Proximal placement of Pd to the Cu sites promotes hydrogenation of the intermediate resulting in high selectivity to hydrogenated chemicals. Anatase TiO_2 catalysts exhibit high advantages for EHRs of organic acids to produce alcoholic compounds due to their sufficiently high CBB level and high overpotential for H_2 evolution. Furthermore, alloying finely tunes the energy states and crystallinity of TiO_2 catalysts to realize highly efficient EHRs. Interestingly, the amino acid synthesis via EHRs of imines and oximes, which are derived from α-keto acids, is achievable by smooth electron transfer using hydrogen bond networks formed on the TiO_2 electrode, i.e., proton-coupled electron transfer. Thus, Hydrogemonics in EHRs is cooperative transport of electrons and protons to reactant molecules, which provides feasible catalytic environment for EHRs.

Multimetallic polyhydride clusters can serve as a unique platform for activation and transformation of small molecules such as N_2 and aromatics due to the synergistic effects of the multiple metal hydride site. In these reactions, hydride ligands play the role of both electron and

proton sources for the reduction, cleavage, and hydrogenation of the reactants, so that no extra reducing agents and proton sources are required. Recently discovered chromium (Group 6 transition metal) hydride clusters bearing sterically demanding cyclopentadienyl ligands revealed high activity toward N_2 via N–N bond cleavage and N–H bond formation. In addition, the titanium hydride clusters bearing the PNP-pincer type ligands was found to cleave N_2 and form N-hetero atom bonds by reacting with a variety of organometallic compounds, revealing many unprecedented aspects of dinitrogen reaction chemistry [62, 63]. In view of these results, investigation of new molecular metal hydride clusters having different metal/ligand combinations will continue to be a significant process for developing efficient molecular systems for small molecule activation and transformation.

Various hydrogenation reactions were demonstrated in this review article. While protiums on metal surfaces and protons/electrons on nanoscale electrocatalysts showed controlled hydrogenations of unsaturated hydrocarbons and CO_2 and reductions of carboxylic acids and α–keto acids, hydrides on multimetallic hydride clusters enabled unprecedented cleavage of N_2 and aromatics under mild conditions. However, whereas the former needs higher reaction rates for the practical application, the latter achieves only stoichiometric reactions and studies on the catalytic systems are still in its infancy. Therefore, continual developments on not only making full use of three hydrogen species, but also utilizing various reaction platforms such as well-designed metal and oxide surfaces, multimetallic clusters, or combination of those are expected to realize more efficient and selective hydrogenation reactions of stable molecules. These works will shed new light on the development of hydrogen science [64] as we call "Hydrogenomics".

Acknowledgements The authors thank support by JSPS KAKENHI Grant-in-Aid for Scientific Research on Innovative Areas "Hydrogenomics" (Grant Nos. JP18H05517, JP18H05518), and Scientific Research (Grant Nos. 20K05534, 21H04650).

References

1. Takagi S, Orimo S-I (2015) Scr Mater 109:1
2. Norton JR, Sowa J (2016) Chem Rev 116:8315
3. Christmann K (1988) Surf Sci Rep 9:1
4. Rhodin TN, Ertl G (eds) (1979) The nature of the surface chemical bond. Elsevier, Amsterdam
5. Li J, Stephanopoulos MF, Xia Y (2020) Chem Rev 120:11699
6. Giannakakis G, Flytzani-Stephanopoulos M, Sykes ECH (2019) Acc Chem Res 52:237
7. Hannagan RT, Giannakakis G, Flytzani-Stephanopoulos M, Sykes ECH (2020) Chem Rev 120:12044
8. Kyriakou G, Boucher MB, Jewell AD, Lewis EA, Lawton TJ, Baber AE, Tierney HL, Flytzani-Stephanopoulos M, Sykes ECH (2012) Science 335:1209
9. Kruppe CM, Krooswyk JD, Trenary M (2017) J Phys Chem C 121:9361
10. O'Connor CR, Duanmu K, Patel DA, Muramoto E, van Spronsen MA, Stacchiola D, Sykes ECH, Sautet P, Madix RJ, Friend CM (2020) Proc Natl Acad Sci USA 117:22657
11. Simonovis JP, Hunt A, Palomino RM, Senanayake SD, Waluyo I (2018) J Phys Chem C 122:4488
12. Simonovis JP, Hunt A, Senanayake SD, Waluyo I (2019) Surf Sci 679:207
13. Namba K, Ogura S, Ohno S, Di W, Kato K, Wilde M, Pletikosić I, Pervan P, Milun M, Fukutani K (2018) Proc Natl Acad Sci USA 115:7896
14. Ceyer ST (2001) Acc Chem Res 34:737
15. Ohno S, Wilde M, Mukai K, Yoshinobu J, Fukutani K (2016) J Phys Chem C 120:11481
16. Ogura S, Okada M, Fukutani K (2013) J Phys Chem C 117:9366
17. Ogura S, Ohno S, Mukai K, Yoshinobu J, Fukutani K (2019) J Phys Chem C 123:7854
18. Horiuti J, Polanyi M (1934) Trans Faraday Soc 30:1164
19. Lloyd L (2011) Handbook of industrial catalysts. Springer, Berlin
20. Olah GA, Goeppert A, Surya Prakash GK (2009) Beyond oil and gas: the methanol economy. Wiley, Weinheim
21. Behrens M, Studt F, Kasatkin I, Kühl S, Hävecker M, Abild-Pedersen F, Zander S, Girgsdies F, Kurr P, Kniep B-L, Tovar M, Fischer RW, Nørskov JK, Schlögl R (2012) Science 336:893
22. Zhong J, Yang X, Wu Z, Liang B, Huang Y, Zhang T (2020) Chem Soc Rev 49:1385
23. Quan J, Muttaqien F, Kondo T, Kozarashi T, Mogi T, Imabayashi T, Hamamoto Y, Inagaki K, Hamada I, Morikawa Y, Nakamura J (2019) Nat Chem 11:722
24. Freund H-J, Roberts M (1996) Surf Sci Rep 25:225
25. Sakaki S, Ohkubo K (1988) Inorg Chem 27:2020
26. Martin O, Martin AJ, Mondelli C, Mitchell S, Segawa TF, Hauert R, Drouilly C, Curulla-Ferre D, Perez-Ramirez J (2016) Angew Chem Int Ed 55:6261
27. Stangeland K, Li H, Yu Z (2020) Energy Ecol Environ 5:272
28. Wang L, Zhang W, Zheng X, Chen Y, Wu W, Qiu J, Zhao X, Zhao X, Dai Y, Zeng J (2017) Nat Energy 2:869
29. Kudo A, Miseki Y (2009) Chem Soc Rev 38:253
30. Watanabe R, Yamauchi M, Sadakiyo M, Abe R, Takeguchi T (2015) Energy Environ Sci 8:1456
31. Fukushima T, Yamauchi M (2019) Chem Commun 55:14721
32. Hori Y, Wakebe H, Tsukamoto T, Koga O (1994) Electrochim Acta 39:1833
33. Dinh C-T, Burdyny T, Kibria MG, Seifitokaldani A, Gabardo CM, García de Arquer FP, Kiani A, Edwards JP, De Luna P, Bushuyev OS, Zou C, Quintero-Bermudez R, Pang Y, Sinton D, Sargent EH (2018) Science 360:783
34. Peterson AA, Norskov JK (2012) J Phys Chem Lett 3:251
35. Sa YJ, Lee CW, Lee SY, Na J, Lee U, Hwang YJ (2020) Chem Soc Rev 49:6632
36. Li J, Sun S (2019) Acc Chem Res 52:2015
37. Yamauchi M, Tsukuda T (2011) Dalton Trans 40:4842
38. Ma S, Sadakiyo M, Heima M, Luo R, Haasch RT, Gold JI, Yamauchi M, Kenis PJA (2017) J Am Chem Soc 139:47
39. Yamauchi M, Hata S, Eguchi H, Kitano S, Fukushima T, Higashi M, Sadakiyo M, Kato K (2019) Catal Sci Technol 9:6561
40. Sadakiyo M, Hata S, Fukushima T, Juhasz G, Yamauchi M (2019) Phys Chem Chem Phys 21:5882
41. Kato K, Tanaka Y, Yamauchi M, Ohara K, Hatsui T (2019) J Synchrotron Radiat 26:762

42. Isegawa M, Staykov A, Yamauchi M (2021) J Phys Chem C 125:12603
43. Tardif O, Nishiura M, Hou Z (2003) Organometallics 22:1171
44. Tardif O, Hashizume D, Hou Z (2004) J Am Chem Soc 126:8080
45. Hou Z, Nishiura M, Shima T (2007) Eur J Inorg Chem 2007:2535
46. Shima T, Hou Z (2016) Recent development in clusters of rare earths and actinides: chemistry and materials. Springer, Berlin, pp 315–336
47. Nishiura M, Hou Z (2010) Nat Chem 2:257
48. Shima T, Hou Z (2017) Dinitrogen fixation by transition metal hydride complexes in nitrogen fixation. Topics in organometallic chemistry. Springer, Berlin, pp 23–43
49. Shima T (2020) J Phys Soc Jpn 89:051014
50. Shima T, Hu S, Luo G, Kang X, Luo Y, Hou Z (2013) Science 340:1549
51. Guru MM, Shima T, Hou Z (2016) Angew Chem Int Ed 55:12316
52. Shima T, Luo G, Hu S, Luo Y, Hou Z (2019) J Am Chem Soc 141:2713
53. Hu S, Shima T, Hou Z (2014) Nature 512:413
54. Kang X, Luo G, Luo L, Hu S, Luo Y, Hou Z (2016) J Am Chem Soc 138:11550
55. Hu S, Luo G, Shima T, Luo Y, Hou Z (2017) Nat Commun 8:1866
56. Hu S, Shima T, Hou Z (2020) J Am Chem Soc 142:19889
57. Fryzuk MD, Johnson SA, Rettig SJ (1998) J Am Chem Soc 120:11024
58. Akagi F, Matsuo T, Kawaguchi H (2007) Angew Chem Int Ed 46:8778
59. Yang J, Luo G, Yu Y, Qu J, Hou Z, Luo Y (2020) Inorg Chem 59:4626
60. Tanaka H, Shiota Y, Matsuo T, Kawaguchi H, Yoshizawa K (2009) Inorg Chem 48:3875
61. Shima T, Yang J, Luo G, Luo Y, Hou Z (2020) J Am Chem Soc 142:9007
62. Wang B, Luo G, Nishiura M, Hu S, Shima T, Luo Y, Hou Z (2017) J Am Chem Soc 139:1818
63. Mo Z, Shima T, Hou Z (2020) Angew Chem Int Ed 59:8635
64. Mohtadi R, Orimo S-I (2016) Nat Rev Mater 2:16091

Authors and Affiliations

K. Fukutani[1,2] · J. Yoshinobu[3] · M. Yamauchi[4,5] · T. Shima[6,7] · S. Orimo[5,8]

1 Institute of Industrial Science, The University of Tokyo, Komaba Meguro-ku, Tokyo 153-8505, Japan

2 Advanced Science Research Center, Japan Atomic Energy Agency (JAEA), Tokai, Ibaraki 319-1195, Japan

3 The Institute for Solid State Physics, The University of Tokyo, Kashiwanoha, Kashiwa, Chiba 277-8581, Japan

4 International Institute for Carbon-Neutral Energy Research (WPI-I2CNER), Kyushu University, Motooka 744, Nishi-ku, Fukuoka 819-0395, Japan

5 Advanced Institute for Materials Research (WPI-AIMR), Tohoku University, 2-1-1 Katahira, Aoba-ku, Sendai 980-8577, Japan

6 Advanced Catalysis Research Group, RIKEN Center for Sustainable Resource Science, Hirosawa, Wako, Saitama 351-0198, Japan

7 Organometallic Chemistry Laboratory, RIKEN Cluster for Pioneering Research, Hirosawa, Wako, Saitama 351-0198, Japan

8 Institute for Materials Research, Tohoku University, 2-1-1 Katahira, Aoba-ku, Sendai 980-8577, Japan